Near-Field Thermophotovoltaic Conversion with High Electrical Power Density and Efficiency above 14%

Christophe Lucchesi, Dilek Cakiroglu, Jean-Philippe Perez, Thierry Taliercio, Eric Tournié, Pierre-Olivier Chapuis, Rodolphe Vaillon

Near-Field Thermophotovoltaic Conversion with High Electrical Power Density and Efficiency above 14%

Christophe Lucchesi,[†] Dilek Cakiroglu,[‡] Jean-Philippe Perez,[‡] Thierry Taliercio,[‡] Eric Tournié,[‡] Pierre-Olivier Chapuis,[†] Rodolphe Vaillon, [‡,†,*]

[†]Univ Lyon, CNRS, INSA-Lyon, Université Claude Bernard Lyon 1, CETHIL UMR5008, F-69621, Villeurbanne, France

[‡]IES, Univ Montpellier, CNRS, Montpellier, France

KEYWORDS: Thermal radiation, nanoscale, thermophotovoltaics, conversion efficiency.

ABSTRACT

A huge amount of thermal energy is available close to material surfaces in radiative and non-radiative states, which can be useful for matter characterization or energy harvesting. Even though a full class of novel nano-engineered devices has been predicted over the last two decades for exploiting near-field thermal photons, efficient near-field thermophotovoltaic conversion could not be achieved experimentally until now. Here, we realize a proof of principle by approaching a micron-sized indium antimonide photovoltaic cell at nanometer distances from a hot (~800 K)

graphite microsphere emitter. We demonstrate conversion efficiency above 14% and unprecedented electrical power density outputs (0.75 $W.cm^{-2}$), orders of magnitude larger than all previous attempts. These results highlight that near-field thermophotovoltaic converters are now competing with other thermal-to-electrical conversion devices such as thermoelectrics and also pave the way for efficient photoelectric detection of near-field thermal photons.

TEXT

A significant number of experimental demonstrations of the enhancement of thermal radiation heat transfer between hot and cold bodies[1–5] establish a firm basis for new nano-engineered devices based on thermal photons in the near field, involving for instance thermal rectification[6] and photonic cooling[7]. In particular, it was predicted 20 years ago that approaching a hot emitter and a photovoltaic cell at nanoscale distances would drastically increase the exchanged thermal radiation, and in turn electrical power generation in the cell[8–10]. Many theoretical results have further elaborated on this idea[11–16]. An early experiment[17] showed qualitative enhancement of the photogeneration of electrical charges at microscale gaps between the emitter and the cell. More recently, three experimental works[18–20] reported on an enhancement of the electrical power in the near field, with estimations of efficiency reaching hardly 1% and a maximal power density of 0.75 $mW.cm^{-2}$. These modest performances indicate that a clear proof of efficient photovoltaic conversion of near-field thermal radiation is still lacking. This is puzzling since ultra-efficient thermophotovoltaics, based on the conversion of radiative heat emitted in the far field, has recently been demonstrated[21,22]. Nevertheless, the electrical power density measured for these far-field devices remains moderate, approaching the $W.cm^{-2}$ level[21,23] only for high-temperature emitters above 1000 °C. The interest for near-field thermophotovoltaic converters, where the transferred

radiative power is much higher, comes from their potential to lead to both significant output power and conversion efficiency[24]. They could also work with heat sources of lower temperatures.

In the present work, we have designed and implemented an experiment to maximize near-field radiative heat-to-electricity conversion from a medium-grade heat source (temperatures in the range 250-650 °C), demonstrating improvements in the three directions (efficiency, power, temperature) and therefore resolving some obstacles to high performance. First, we have used a configuration improving the view factor between the emitter and the photovoltaic cell. In the present case, it involves a spherical emitter exchanging radiation with a planar receiver[1,2,25–28], which allows to scan a large emitter-cell distance range, from millimeters down to nanometers, to highlight the strong advantage of near field for the output power. Second, we have used photovoltaic cells with specific architectures for collecting efficiently near-field photons. They are made of indium antimonide (InSb), having a very low bandgap energy (0.23 eV, *i.e.* 5.3 μm, at 77 K) particularly well suited for converting mid-infrared photons typical for thermal radiation. Finally, we have identified cell design parameters that allow the maximization of electrical power density and conversion efficiency.

The experimental set-up (see Fig. 1) is made of a hot micron-sized spherical emitter (Fig. 1b) and a micron-sized photovoltaic cell (view from top in Fig. 1c), separated by a distance that can be varied. It allows measuring both the radiative power exchanged between them and the electrical power generated by the cell, as a function of the emitter-cell distance. Let us start by detailing the photovoltaic cell. A key feature is that it is specifically designed for harvesting thermal radiation fluxes of medium-grade temperature sources, around 500 °C, in the near field[29]. It is a *p-n* junction (Fig. 1a) made of InSb, one of the III-V semiconductors with the longest bandgap wavelength. The cell can thus convert photons with wavelengths in the micrometer range (Fig. 1d). The bandgap

wavelength depends on temperature and varies from 5.3 µm at 77 K to 7.3 µm at room temperature. The architecture of the cell was optimized based on full calculations involving the coupling of charge transport and radiative absorption in a 1D configuration[29]. The *p-n* junction is located close to the cell top-surface (a few hundreds of nanometers only) to collect a large share of the near-field photons. The size of the cell has to match that of the emitter to avoid unilluminated zones, which are detrimental to electrical performances. Thus, the cell active area is a few tens of micrometers in diameter in order to optimize the view factor (see Supplementary Section 1 and Fig. 7a). Gold layers are used as top and bottom electrical contacts. It is important to underline that InSb can operate as a proper *p-n* junction at low temperature only[30], so in this experiment the cell is cooled down to 77 K by placing it on the cold finger of a cryostat located in a vacuum chamber (see Supplementary Section 1).

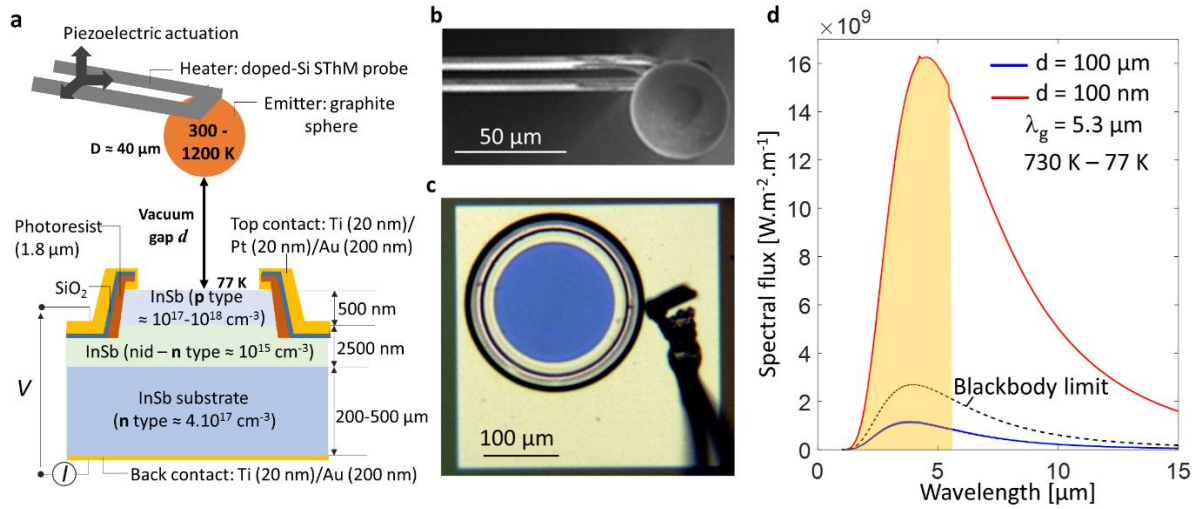

Figure 1. Device and simulated radiative heat transfer for near-field thermophotovoltaic conversion. (a) Scheme of the spherical emitter-planar photovoltaic cell device. (b) Scanning electron micrograph of the emitter seen from below. A graphite sphere is glued on the tip of a SThM doped-Si probe with a ceramic adhesive. (c) Optical microscopy top view of an InSb cell. (d) Simulated thermal radiation heat transfer spectrum for the case of a 732 K emitter and 77 K cell for far-field (blue curve) and near-field (red curve) configurations.

The emitter is a graphite microsphere. It is glued to the probe of a scanning thermal microscope (SThM, see Fig. 1c), which is an atomic force microscope (AFM) where a temperature sensor is located on the cantilever[31]. It allows measuring the emitted radiative heat flux. The resistive sensor is made of doped silicon, the evolution of which as a function of temperature is known. The temperature of the sphere is estimated to be equal to that of the resistor. The thermal conductance from the tip temperature to the ambient was measured, which allowed monitoring variations of the radiative flux lost by the emitter (see Supplementary Section 1 and Fig. 1). Most of the results presented here were obtained for a tip apex temperature of 732 K (439 °C), which maximizes measurement sensitivity, but the emitter could be heated up to temperatures larger than 1200 K. Graphite was selected for the emitter as the material maximizing the near-field radiative exchange with InSb (Supplementary Fig. 2). Fig. 1(d) indicates that about 40% of the overall power exchanged between a planar emitter and a planar receiver is located in the wavelength range that can be converted to electricity. It also shows that reducing the distance between the emitter and the cell strongly increases radiative exchange. Still, we selected a spherical emitter, despite its reduced near-field exchange with respect to a planar one at the same distance (Supplementary Fig. 2c), to eliminate parallelism issues inherent to planar configurations. In the experiment, a spherical emitter is therefore approached in the vicinity of the cell by moving it vertically with a piezo-actuator. Such geometry was successful for Casimir force and near-field radiative heat flux experiments^{1,2,25–28,31} and allows probing a large emitter-cell distance range, from the sub-100 nm region to millimeters.

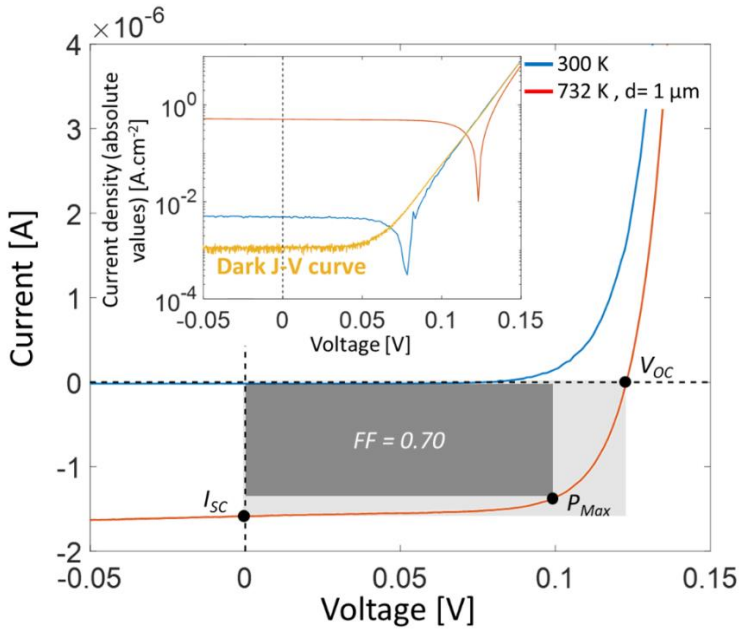

Figure 2. Current-voltage characteristics of a cell at 77 K having a 20 µm active area diameter. I-V curves (single realizations) under 300 K ambient illumination (blue), 732 K graphite sphere at d = 1 µm (red) and under dark conditions (orange, inset). The dark and light gray rectangles represent respectively the maximum output power configuration and the product V_{OC} I_{SC}, used for computation of the fill factor (FF). The inset shows the current density in absolute values according to the applied voltage. The curves were obtained for a 500 µm-thick InSb substrate and a 10^{17} cm^{-3} p-doping level. The observed noise (standard deviation, see e.g. dark J-V curve) is 3.5 10^{-10} A.

The cells (maintained at 77 K) are first characterized (Fig. 2). I-V curves in the dark indicate a low noise level (mA.cm^{-2}) in the experiments. Remarkably, room-temperature radiative (far-field) emission leads to a significant electrical power generation by the cell. The open-circuit voltage depends on the temperature of the emission source (see diverging values in the logarithmic scale of the inset of Fig. 2) and is found to be larger than 100 mV, which is around half the bandgap energy of InSb (E_g = 0.23 eV), for a source at 732 K and located at d = 1 µm from the cell. In contrast to previous reports[19,20], the I-V curves look like typical photovoltaic cell characteristics, i.e. rectangles with a rounded corner. The short-circuit currents depend on the emitter temperature

and emitter-cell distance and reach already microamps at 1 μm. Fill factors are as high as 0.75, leading to electrical output powers up to 5.5 μW, depending on the distance.

The high sensitivity of the electrical power output measurement allows following the approach of the hot sphere towards the cold cell from distances up to millimeters. The evolution of the short-circuit current with the emitter-sphere distance superimposes nicely the prediction of far-field view factor theory for these large distances (inset in Fig. 3b and Supplementary Fig. 8b). This indicates that far-field thermophotovoltaic conversion depends only on the level of illumination.

We now focus on the near field, which is approximately defined by the distance range below Wien's wavelength ($\lambda_W.T$= 2898 μm.K) for the emitter, *i.e.* below 4 μm. Our setup allows the measurement of the radiative exchange as a function of the emitter-cell distance and the increase of the current-voltage curve at the same time. As expected, a strong enhancement of the flux is observed for small distances, where the exchanged radiative power variation reaches 7.4 μW. Almost all of this increase is due to the near-field contribution, since the gain from the far-field contribution is much weaker in the last micrometers. While we cannot directly measure the far-field contribution background, it is computed to be ~3.2 μW for a sphere at 732 K and a cell having a 20 μm active area diameter (Supplementary Section 5).

The electrical output power at the maximum power point (Fig. 3b), red curve) is derived from measurements of I-V curves as a function of emitter-cell distance at the same time as the radiative flux data (Fig. 3a, blue curve). It reaches almost 1.3 μW at the smallest distance for the selected case, leading to an overall efficiency estimated to be about 12%. This is one order of magnitude higher than the best previous experiment[18]. It is noticeable that such a value competes with the efficiency of state-of-the-art thermoelectrics[32,33]. It is interesting to estimate the contribution of the

near field to this power increase. By matching the view factor computation as a function of distance to the largest distances in the curve (dashed-dotted black curve in Fig. 3b), we are able to single out a stronger increase of the electrical output power in the sub-3 µm region than what standard far-field theory predicts (yellow region). An electrical output power 4.6 times larger than the far-field one is found.

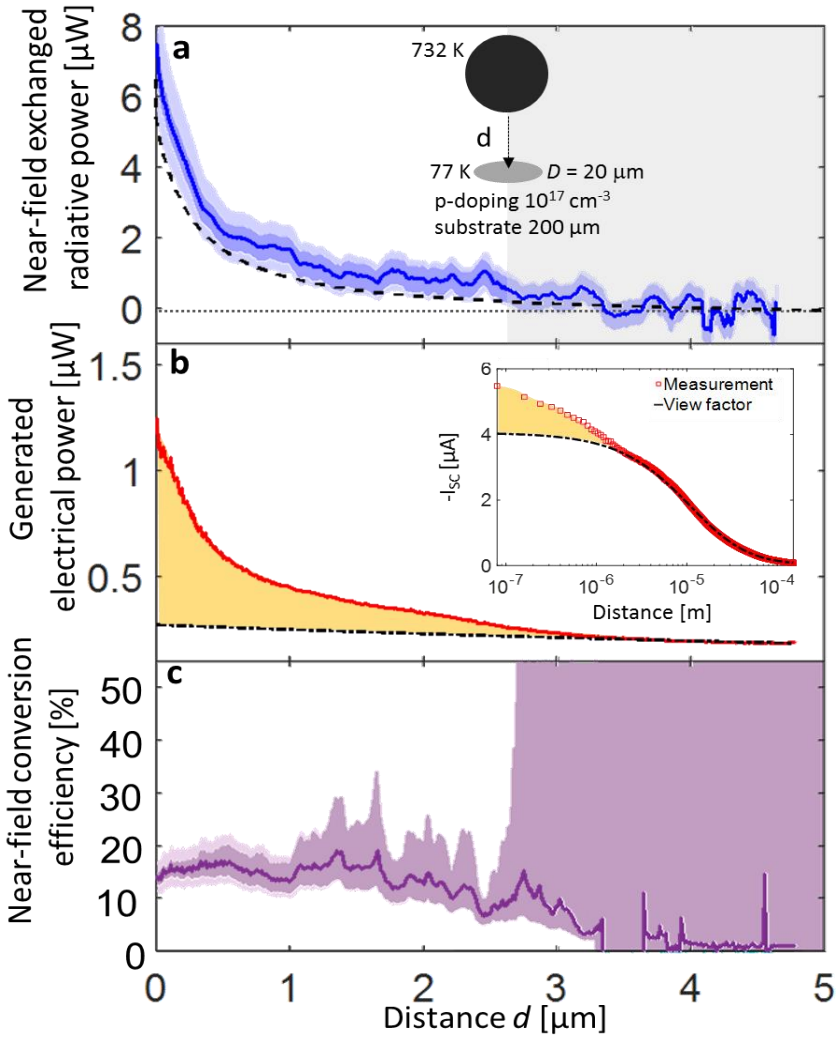

Figure 3. Near-field exchanged radiative power, maximum generated electrical power and near-field conversion efficiency obtained simultaneously as a function of emitter-cell distance. (a) Near-field radiative power according to distance. Measurements (blue curve) are compared with calculations (dark-dashed curve) performed in the frame of the proximity approximation. (b) Generated electrical power, deduced

from the measurement of I-V curves as a function of distance. The total electrical power (red curve) is compared to the power increase due to the far-field contribution estimated from the view factor (dashed-dotted black curve). The region between the two curves provides the near-field electrical power. The inset data, obtained with another cell, show the match between the view factor computation (plain line) and the experimental data in the far field. (c) Near-field conversion efficiency calculated by dividing the near-field electrical power (b) by the near-field exchanged radiative power (a). The dark-shaded zones around the mean curve correspond to the standard deviation (SD) (17 measurements in the small-distance regime, with a decaying number when distance is increased, leading to a larger SD). The small SD (<1%) in panel (b) is not represented. The light-shaded zones represent the systematic relative uncertainty of 20 % induced by the calibration of the emitter.

Photovoltaic conversion efficiency of the near-field flux can be determined from the experimental data as a function of emitter-cell distance in the range from contact to 2 μm. By dividing the electrical power by the near-field radiation power, we find a near-field conversion efficiency of the order of 14-19% for this distance range (Fig. 3c); uncertainty is linked to the near-field radiation data). The distance is measured by the vertical piezoelectric actuator, with an uncertainty close to the contact up to around 80 nm (Supplementary Fig. 6).

Parameters that can improve radiative heat-to-electricity conversion are now analyzed. We underline that the near-field contribution in the sphere-plane geometry is mostly related to optical modes that are evanescent in the gap but propagate in the substrate ("frustrated modes", see Supplementary Figs. 4 and 5). First, the effect of the diameter of the active area of the cell is reported in Fig. 4a. As a larger share of the exchanged power comes from the near field for the smallest cell (dark orange region), it performs the best, being able to generate about 2 $kW.m^{-2}$, which is three orders of magnitude higher than previous reports[18–20]. The influence of two other parameters predicted to be critical is analyzed in Fig. 4b, namely the substrate thickness and the doping concentration of the p-region of the junction[29]. When the substrate thickness is decreased from 500 μm to 200 μm (Fig. 4b-left), a clear enhancement of the power output is observed in the

experiment. By thinning down the substrate of the cell, the near-field efficiency is more than doubled and reaches 14.1% (see Supplementary Tab. 1 and Section 11). Anterior theoretical analyses in 1D predicted that this effect would occur because of lower absorption below the bandgap[29,34] and higher absorption above the bandgap[29]. Measurements show that the efficiency enhancement is the result of a rise in electrical power without any substantial change in the net radiative flux exchanged. 2D effects on radiative transfer and electrical charges transport, and impact of the emitter on external luminescence of the cell[35] can be invoked as possible other explanations. Finally, an impressive 4-fold enhancement of the electrical power is observed (Fig. 4b-right) when increasing the p-region dopant concentration from 10^{17} to 10^{18} cm^{-3}, leading to a record 7.5 $kW.m^{-2}$ value for the tested micron-sized cells, despite the moderate temperature of the emitter (432 °C).

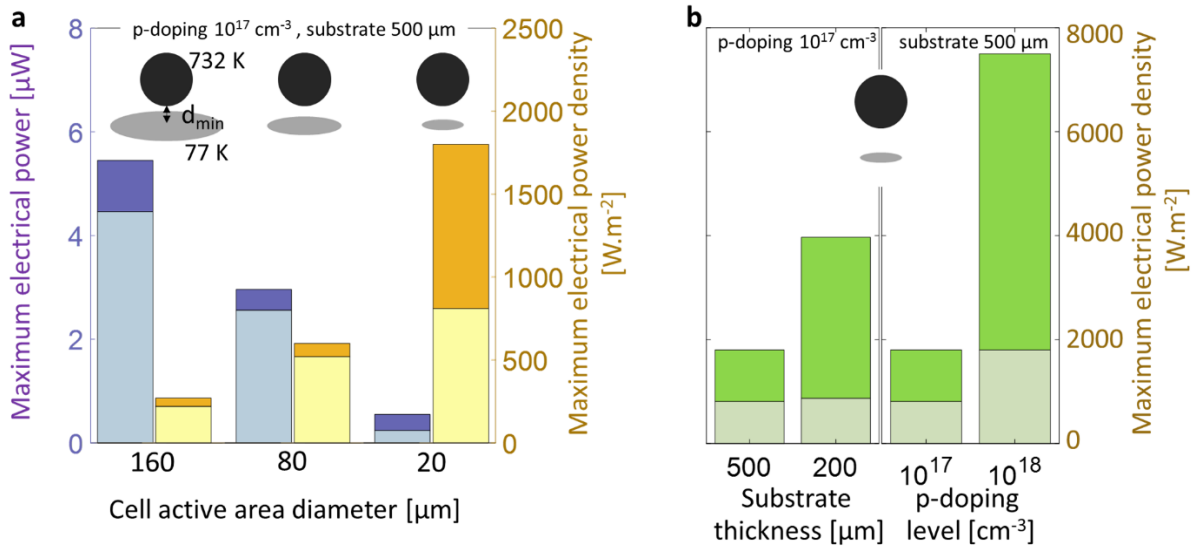

Figure 4. Influence of cell diameter, substrate thickness and p-doping level on the maximum electrical power for the smallest emitter-cell distances. The dark and light parts are respectively the far-field and near-field contributions. (a) Influence of the cell active area diameter. The electrical power decreases with the cell diameter because less illumination is collected, but the electrical power density increases. (b) (left) Influence of the substrate thickness. The maximum electrical power density is observed for the device with

the thinnest substrate. (right) Influence of the p-doping level. The maximum power density increases with the doping level. The standard deviations are small (less than 1%) and therefore not represented.

In summary, we have measured photovoltaic conversion of thermal photons in the near field with efficiency above 14% and electrical power densities reaching 0.75 $W.cm^{-2}$, close to the ~1 $W.cm^{-2}$ threshold typical for powerful energy harvesting devices[36] and close to the best far-field thermophotovoltaic performances despite much lower emitter temperatures[21,23]. The present approach highlights the possibility of using the photocurrent as signal for characterization purposes, converting the photons directly close to the surface and therefore acquiring the signature of the sample with superior sensitivity. For energy harvesting as in solar thermophotovoltaics[37–39], it is also required to upscale the sizes and to avoid cooling the cell. Our architectures are compatible with more industrial-size implementations involving parallel flat surfaces that were undertaken recently[40]. Recent strategies for designing efficient far-field cells with narrow energy bandgap III-V materials operating at room temperature[41] can also be applied in the near field with frustrated photon modes and will be particularly useful for harnessing energy of medium-grade heat sources. For high-grade heat sources, we have demonstrated the possibility to maintain a temperature difference larger than 1100 K across a small distance (Supplementary Fig. 10), so higher energy bandgap materials used in cells operating at room temperature could also be considered with a careful design for the near field following the highlighted paths. Finally, it is reminded that further enhancement of the performances is predicted for materials with polariton resonances above the energy bandgap[11,12]. This work thus opens the door to efficient exploitation of near-field thermal photons.

ASSOCIATED CONTENT

Supporting Information

The Supporting Information is available free of charge. (1) Main experimental methods. (2) Selection of the emitter material. (3) Sphere-plane vs. plane-plane configurations. (4) Comparison between near-field thermal radiative measurements and the proximity approximation. (5) Contribution of the propagating modes with distance. (6) Numerical analysis of the near-field modes and radiative absorption as a function of depth. (7) Estimation of the sphere-cell distance close to contact. (8) Characterization of the photovoltaic cells. (9) Validation of the superposition principle. (10) Impact of emitter temperature on power output. (11) Impact of emitter temperature on power output. (12) I-V characteristics and efficiency according to distance. (13) Summary of the results.

AUTHOR INFORMATION

Corresponding Author

*E-mail: rodolphe.vaillon@ies.univ-montp2.fr

Author Contributions

R.V., P-O.C, J-P.P., E.T. and T.T. conceived and supervised the work. J-P.P. did the MBE growth of the InSb material and D.C. fabricated the photovoltaic cells. C.L. fabricated the emitter and performed the experiments. C.L. and R.V. performed the simulations. The manuscript was written by C.L., P-O.C and R.V. with comments and inputs from all authors.

Funding Sources

Financial support by the French National Research Agency (ANR) under grant No. ANR-16-CE05-0013 and partial funding by the French "Investment for the Future" program (EquipEx EXTRA ANR-11-EQPX-0016 and IDEXLYON ANR-16-IDEX-0005) and by the Occitanie region are acknowledged.

Notes

The authors declare no competing financial interest.

ACKNOWLEDGMENT

C.L. and P.O.C. thank C. Ducat, N. Pouchot and A. Buthod for help in the design of the setup, P. Mangel and D. Renahy for experimental support, and S. Gomès. P.O.C thanks S. Volz for equipment handover.

REFERENCES

(1) Narayanaswamy, A.; Shen, S.; Chen, G. Near-Field Radiative Heat Transfer between a Sphere and a Substrate. *Phys. Rev. B* **2008**, *78* (11), 115303. https://doi.org/10.1103/PhysRevB.78.115303.

(2) Rousseau, E.; Siria, A.; Jourdan, G.; Volz, S.; Comin, F.; Chevrier, J.; Greffet, J. J. Radiative Heat Transfer at the Nanoscale. *Nat. Photonics* **2009**, *3* (9), 514–517. https://doi.org/10.1038/nphoton.2009.144.

(3) Lim, M.; Lee, S. S.; Lee, B. J. Near-Field Thermal Radiation between Doped Silicon Plates at Nanoscale Gaps. *Phys. Rev. B* **2015**, *91* (19). https://doi.org/10.1103/PhysRevB.91.195136.

(4) Bernardi, M. P.; Milovich, D.; Francoeur, M. Radiative Heat Transfer Exceeding the Blackbody Limit between Macroscale Planar Surfaces Separated by a Nanosize Vacuum Gap. *Nat. Commun.* **2016**, *7* (1), 12900. https://doi.org/10.1038/ncomms12900.

(5) Watjen, J. I.; Zhao, B.; Zhang, Z. M. Near-Field Radiative Heat Transfer between Doped-Si Parallel Plates Separated by a Spacing down to 200 Nm. *Appl. Phys. Lett.* **2016**, *109* (20), 203112. https://doi.org/10.1063/1.4967384.

(6) Fiorino, A.; Thompson, D.; Zhu, L.; Mittapally, R.; Biehs, S.-A.; Bezencenet, O.; El-

Bondry, N.; Bansropun, S.; Ben-Abdallah, P.; Meyhofer, E.; Reddy, P. A Thermal Diode Based on Nanoscale Thermal Radiation. *ACS Nano* **2018**, *12* (6), 5774–5779. https://doi.org/10.1021/acsnano.8b01645.

(7) Zhu, L.; Fiorino, A.; Thompson, D.; Mittapally, R.; Meyhofer, E.; Reddy, P. Near-Field Photonic Cooling through Control of the Chemical Potential of Photons. *Nature* **2019**, *566* (7743), 239–244. https://doi.org/10.1038/s41586-019-0918-8.

(8) Pan, J. L.; Choy, H. K. H.; Fonstad, C. G. Very Large Radiative Transfer over Small Distances from a Black Body for Thermophotovoltaic Applications. *IEEE Trans. Electron Devices* **2000**, *47* (1), 241–249. https://doi.org/10.1109/16.817591.

(9) Whale, M. D.; Cravalho, E. G. Modeling and Performance of Microscale Thermophotovoltaic Energy Conversion Devices. *IEEE Trans. Energy Convers.* **2002**, *17* (1), 130–142. https://doi.org/10.1109/60.986450.

(10) Mulet, J.-P.; Joulain, K.; Carminati, R.; Greffet, J.-J. Enhanced Radiative Heat Transfer at Nanometric Distances. *Microscale Thermophys. Eng.* **2002**, *6* (3), 209–222. https://doi.org/10.1080/10893950290053321.

(11) Laroche, M.; Carminati, R.; Greffet, J. J. Near-Field Thermophotovoltaic Energy Conversion. *J. Appl. Phys.* **2006**, *100* (6), 063704. https://doi.org/10.1063/1.2234560.

(12) Narayanaswamy, A.; Chen, G. Surface Modes for near Field Thermophotovoltaics. *Appl. Phys. Lett.* **2003**, *82* (20), 3544. https://doi.org/10.1063/1.1575936.

(13) Francoeur, M.; Vaillon, R.; Meng, M. P. Thermal Impacts on the Performance of Nanoscale-Gap Thermophotovoltaic Power Generators. *IEEE Trans. Energy Convers.* **2011**, *26* (2). https://doi.org/10.1109/TEC.2011.2118212.

(14) Jin, S.; Lim, M.; Lee, S. S.; Lee, B. J. Hyperbolic Metamaterial-Based near-Field

Thermophotovoltaic System for Hundreds of Nanometer Vacuum Gap. *Opt. Express* **2016**, *24* (6), A635. https://doi.org/10.1364/oe.24.00a635.

(15) Ben-Abdallah, P.; Biehs, S. A. Harvesting the Electromagnetic Energy Confined Close to a Hot Body. *Zeitschrift fur Naturforsch. - Sect. A J. Phys. Sci.* **2019**, *74*, 689–696.

(16) St-Gelais, R.; Bhatt, G. R.; Zhu, L.; Fan, S.; Lipson, M. Hot Carrier-Based Near-Field Thermophotovoltaic Energy Conversion. *ACS Nano* **2017**, *11* (3), 3001–3009. https://doi.org/10.1021/acsnano.6b08597.

(17) DiMatteo, R. S.; Greiff, P.; Finberg, S. L.; Young-Waithe, K. A.; Choy, H. K. H.; Masaki, M. M.; Fonstad, C. G. Enhanced Photogeneration of Carriers in a Semiconductor via Coupling across a Nonisothermal Nanoscale Vacuum Gap. *Appl. Phys. Lett.* **2001**, *79* (12), 1894–1896. https://doi.org/10.1063/1.1400762.

(18) Inoue, T.; Koyama, T.; Kang, D. D.; Ikeda, K.; Asano, T.; Noda, S. One-Chip Near-Field Thermophotovoltaic Device Integrating a Thin-Film Thermal Emitter and Photovoltaic Cell. *Nano Lett.* **2019**, *19* (6), 3948–3952. https://doi.org/10.1021/acs.nanolett.9b01234.

(19) Fiorino, A.; Zhu, L.; Thompson, D.; Mittapally, R.; Reddy, P.; Meyhofer, E. Nanogap Near-Field Thermophotovoltaics. *Nat. Nanotechnol.* **2018**, *13* (9), 806–811. https://doi.org/10.1038/s41565-018-0172-5.

(20) Bhatt, G. R.; Zhao, B.; Roberts, S.; Datta, I.; Mohanty, A.; Lin, T.; Hartmann, J.-M.; St-Gelais, R.; Fan, S.; Lipson, M. Integrated Near-Field Thermo-Photovoltaics for Heat Recycling. *Nat. Commun.* **2020**, *11*, 2545.

(21) Omair, Z.; Scranton, G.; Pazos-Outón, L. M.; Xiao, T. P.; Steiner, M. A.; Ganapati, V.; Peterson, P. F.; Holzrichter, J.; Atwater, H.; Yablonovitch, E. Ultraefficient Thermophotovoltaic Power Conversion by Band-Edge Spectral Filtering. *Proc. Natl. Acad.*

Sci. U. S. A. **2019**, *116* (31), 15356–15361. https://doi.org/10.1073/pnas.1903001116.

(22) Fan, D.; Burger, T.; McSherry, S.; Lee, B.; Lenert, A.; Forrest, S. R. Near-Perfect Photon Utilization in an Air-Bridge Thermophotovoltaic Cell. *Nature* **2020**, No. February. https://doi.org/10.1038/s41586-020-2717-7.

(23) Wernsman, B.; Siergiej, R. R.; Link, S. D.; Mahorter, R. G.; Palmisiano, M. N.; Wehrer, R. J.; Schultz, R. W.; Schmuck, G. P.; Messham, R. L.; Murray, S.; Murray, C. S.; Newman, F.; Taylor, D.; DePoy, D. M.; Rahmlow, T. Greater than 20% Radiant Heat Conversion Efficiency of a Thermophotovoltaic Radiator/Module System Using Reflective Spectral Control. *IEEE Trans. Electron Devices* **2004**, *51* (3), 512–515. https://doi.org/10.1109/TED.2003.823247.

(24) Okanimba Tedah, I. A.; Maculewicz, F.; Wolf, D. E.; Schmechel, R. Thermoelectrics versus Thermophotovoltaics: Two Approaches to Convert Heat Fluxes into Electricity. *J. Phys. D. Appl. Phys.* **2019**, *52* (27), 275501. https://doi.org/10.1088/1361-6463/ab1833.

(25) Shen, S.; Narayanaswamy, A.; Chen, G. Surface Phonon Polaritons Mediated Energy Transfer between Nanoscale Gaps. *Nano Lett.* **2009**, *9* (8), 2909–2913. https://doi.org/10.1021/nl901208v.

(26) Song, B.; Ganjeh, Y.; Sadat, S.; Thompson, D.; Fiorino, A.; Fernández-Hurtado, V.; Feist, J.; Garcia-Vidal, F. J.; Cuevas, J. C.; Reddy, P.; Meyhofer, E. Enhancement of Near-Field Radiative Heat Transfer Using Polar Dielectric Thin Films. *Nat. Nanotechnol.* **2015**, *10* (3), 253–258. https://doi.org/10.1038/nnano.2015.6.

(27) Shi, J.; Liu, B.; Li, P.; Ng, L. Y.; Shen, S. Near-Field Energy Extraction with Hyperbolic Metamaterials. *Nano Lett.* **2015**, *15* (2), 1217–1221. https://doi.org/10.1021/nl504332t.

(28) Menges, F.; Dittberner, M.; Novotny, L.; Passarello, D.; Parkin, S. S. P.; Spieser, M.; Riel,

H.; Gotsmann, B. Thermal Radiative near Field Transport between Vanadium Dioxide and Silicon Oxide across the Metal Insulator Transition. *Appl. Phys. Lett.* **2016**, *108* (17), 171904. https://doi.org/10.1063/1.4948364.

(29) Vaillon, R.; Pérez, J.-P.; Lucchesi, C.; Cakiroglu, D.; Chapuis, P.-O.; Taliercio, T.; Tournié, E. Micron-Sized Liquid Nitrogen-Cooled Indium Antimonide Photovoltaic Cell for near-Field Thermophotovoltaics. *Opt. Express* **2019**, *27* (4), A11. https://doi.org/10.1364/oe.27.000a11.

(30) Cakiroglu, D.; Perez, J.-P.; Evirgen, A.; Lucchesi, C.; Chapuis, P.-O.; Taliercio, T.; Tournié, E.; Vaillon, R. Indium Antimonide Photovoltaic Cells for Near-Field Thermophotovoltaics. *Sol. Energy Mater. Sol. Cells* **2019**, *203*, 110190. https://doi.org/10.1016/j.solmat.2019.110190.

(31) Gomès, S.; Assy, A.; Chapuis, P. O. Scanning Thermal Microscopy: A Review. *Phys. Status Solidi Appl. Mater. Sci.* **2015**, *212* (3), 477–494.

(32) Datas, A.; Martí, A. Thermophotovoltaic Energy in Space Applications: Review and Future Potential. *Sol. Energy Mater. Sol. Cells* **2017**, *161*, 285–296. https://doi.org/10.1016/J.SOLMAT.2016.12.007.

(33) He, J.; Tritt, T. M. Advances in Thermoelectric Materials Research: Looking Back and Moving Forward. *Science (80-.).* **2017**, *357* (6358), eeak9997.

(34) Chen, K.; Santhanam, P.; Fan, S. Suppressing Sub-Bandgap Phonon-Polariton Heat Transfer in near-Field Thermophotovoltaic Devices for Waste Heat Recovery. *Appl. Phys. Lett.* **2015**, *107* (9), 091106. https://doi.org/10.1063/1.4929949.

(35) Desutter, J.; Vaillon, R.; Francoeur, M. External Luminescence and Photon Recycling in Near-Field Thermophotovoltaics. *Phys. Rev. Appl.* **2017**, *8* (1).

https://doi.org/10.1103/PhysRevApplied.8.014030.

(36) Shirvanimoghaddam, M.; Shirvanimoghaddam, K.; Abolhasani, M. M.; Farhangi, M.; Zahiri Barsari, V.; Liu, H.; Dohler, M.; Naebe, M. Towards a Green and Self-Powered Internet of Things Using Piezoelectric Energy Harvesting. *IEEE Access* **2019**, *7*, 94533–94556. https://doi.org/10.1109/ACCESS.2019.2928523.

(37) Bierman, D. M.; Lenert, A.; Chan, W. R.; Bhatia, B.; Celanović, I.; Soljačić, M.; Wang, E. N. Enhanced Photovoltaic Energy Conversion Using Thermally Based Spectral Shaping. *Nat. Energy* **2016**, *1*, 16068. https://doi.org/10.1038/nenergy.2016.68.

(38) Ungaro, C.; Gray, S. K.; Gupta, M. C. Solar Thermophotovoltaic System Using Nanostructures. *Opt. Express* **2015**, *23* (19), A1149. https://doi.org/10.1364/OE.23.0A1149.

(39) Shimizu, M.; Kohiyama, A.; Yugami, H. High-Efficiency Solar-Thermophotovoltaic System Equipped with a Monolithic Planar Selective Absorber/Emitter. *J. Photonics Energy* **2015**, *5*, 053099. https://doi.org/10.1117/1.JPE.5.053099.

(40) DeSutter, J.; Tang, L.; Francoeur, M. A Near-Field Radiative Heat Transfer Device. *Nat. Nanotechnol.* **2019**, *14* (8), 751–755. https://doi.org/10.1038/s41565-019-0483-1.

(41) Huang, W.; Lei, L.; Li, L.; Massengale, J. A.; Yang, R. Q.; Mishima, T. D.; Santos, M. B. Enhanced Collection Efficiencies and Performance of Interband Cascade Structures for Narrow Bandgap Semiconductor Thermophotovoltaic Devices. *J. Appl. Phys.* **2018**, *124* (2), 023101. https://doi.org/10.1063/1.5030904.